ELSEVIER

Journal of Nuclear Materials 282 (2000) 159–170

journal of nuclear materials

www.elsevier.nl/locate/jnucmat

The EFTTRA-T4 experiment on americium transmutation

R.J.M. Konings [a,*], R. Conrad [b], G. Dassel [c], B.J. Pijlgroms [c], J. Somers [a], E. Toscano [a]

[a] *European Commission, Joint Research Centre, Institute for Transuranium Elements, Postfach 2340, D-76125 Karlsruhe, Germany*
[b] *European Commission, Joint Research Centre, Institute for Advanced Materials, P.O. Box 2, NL-1755 ZG Petten, The Netherlands*
[c] *NRG, P.O. Box 25, NL-1755 ZG, Petten, The Netherlands*

Received 22 May 2000; accepted 8 September 2000

Abstract

In the EFTTRA-T4 experiment the irradiation behaviour of a target containing americium dispersed in $MgAl_2O_4$ was studied. Pellets containing 10–12 wt% ^{241}Am were fabricated by the infiltration method. However, it was found that the americium, intended to be present as AmO_{2-x}, formed a compound, probably $AmAlO_3$, during sintering. The T4 target was irradiated in the High Flux Reactor (HFR) Petten from August 1996 to January 1998 (358.4 fpd's). Post-test burn-up calculations indicated that the ^{241}Am concentration is reduced to 4% of the initial value at the end of the irradiation. The fraction of the initial americium atoms that were fissioned is 28%. Non-destructive and destructive examinations of the target indicated that swelling of the target pellets occurred. This is attributed to accumulation of helium, produced by alpha decay of ^{242}Cm that occurs in the transmutation scheme of ^{241}Am.

1. Introduction

The radiotoxic inventory of spent fuel from nuclear reactors remains relatively high during the period of 250 to 100 000 years of storage due to the presence of long-lived isotopes of plutonium and the minor actinides. These isotopes are formed as a result of subsequent neutron capture and alpha- or beta-decay reactions, mainly starting from the ^{238}U isotope. The plutonium isotopes contribute for about 90% to the radiotoxic inventory, the remaining 10% being mainly due to americium and curium. In the high-level waste arising from reprocessing activities, during which 99.88% of the plutonium and uranium are recovered, americium and curium are the main contributors. Partitioning and transmutation of americium (and curium) are therefore considered a possible extension of the current recycling strategy when a significant reduction of the radiotoxic inventory of the high-level waste is the aim.

Partitioning in this context means the separation of americium from the high-active raffinate generated during reprocessing by the PUREX process. It is being investigated extensively in Europe and major advances have been made [1]. Several processes that are being studied on a laboratory scale show good performance and there is confidence that they can be developed on an industrial scale.

Transmutation of americium means the conversion of long-lived isotopes to short-lived or stable ones. It is a complex process of neutron capture, fission and decay reactions. Neutron capture and decay reactions lead to the formation of other actinides and only the fission reactions effectively destroy the americium. To reach a considerable reduction of the radiotoxicity, at least 90% of the americium needs to be fissioned. This can be achieved by multiple recycling in a fast neutron flux or once-through transmutation in a high-thermal or epithermal neutron flux [2]. Multiple recycling is only feasible if small losses in the partitioning process can be achieved and if the hazardous ^{238}Pu and ^{242}Cm isotopes can be recycled. Once-through transmutation requires long irradiation times and, consequently, extreme requirements for fuel and cladding materials.

* Corresponding author. Tel.: +49-7247 951 391; fax:+49-7247 951 566.
E-mail address: konings@itu.fzk.de (R.J.M. Konings).

0022-3115/00/$ - see front matter
PII: S0022-3115(00)00411-6

It is generally accepted that the mixing of americium in small quantities in UO_2 or MOX fuel (homogeneous recycling) is not preferred because it has a large impact on the fuel cycle [2]. Radiological protection is needed for the fabrication of such fuel due to gamma emission and reprocessing is complicated due to heat production and neutron emission. As only small amounts of americium can be added to MOX fuel, the number of americium-containing subassemblies would be relatively high. In addition, the impact on the core reactivity coefficients is considerable. Heterogeneous recycling in an inert-matrix fuel (IMF) or target, in which a ceramic material serves as a support for the actinide phase to keep a good mechanical integrity of the target during irradiation, is therefore preferred. The number of IMF subassemblies required for the same mass throughput is much less than that for homogeneous recycling concepts. In addition, the impact on the core reactivity can be reduced by placing the IMF subassembly at the core periphery or optimising the design of the subassembly.

In the present paper, the results of an experimental pilot study of the transmutation of americium in an inert-matrix target (ceramic–ceramic or CERCER type) are presented. The aim of the experiment was the investigation of the technical feasibility of the inert-matrix concept with the emphasis on the materials aspects. Due to the selection of the inert matrix (magnesium aluminate spinel), which is not compatible with the PUREX process (it is insoluble in nitric acid), and the characteristics of the reactor (the High Flux Reactor (HFR) at Petten), the experiment is representative for a once-through scenario in an (epi)thermal neutron flux. The project activities included the fabrication of the targets, the irradiation and the post-irradiation examination of the target. The project was performed by the members of the Experimental Feasibility of Targets for Transmutation (EFTTRA) group, and is named EFTTRA-T4. EFTTRA is a network of research organisations in France (EdF and CEA), Germany (JRC-ITU and FZK) and the Netherlands (JRC-IAM and NRG) and was formed in 1992 to study the transmutation of both americium and long-lived fission products technetium (^{99}Tc) and iodine (^{129}I) [3,4].

2. Experimental

2.1. Sample preparation

The EFTTRA-T4 sample was prepared by infiltration of porous $MgAl_2O_4$ pellets with an americium nitrate solution according to the methods described in [5]. The porous pellets were prepared from a commercial powder (Baikalox S33CR, Baikowski Chemie) that was granulated and compacted at a pressure of 390 MPa using a bi-directional press. The resulting pellets were thermally treated at 650°C to remove zinc stearate that was used as a lubricant in the pressing step. The resulting pellets had a diameter of 6.5 mm, heights between 8 and 9 mm and a porosity of 49%.

The pellets were placed in batches (up to 12) on a perforated teflon tray, which was lowered slowly into an Am nitrate solution, that was prepared by dissolving americium oxide in nitric acid and concentrated to an Am metal content of approximately 400 g/l. The pellets were maintained under the surface of the liquid for at least 10 min. Upon withdrawal they were dried, and then calcined at 700°C for 4 h under Ar/H_2 before being sintered at 1650°C under the same atmosphere. The sintered pellets had a diameter of 5.39 ± 0.03 mm and their densities were $96.5 \pm 0.5\%$ of the theoretical value. However, it was found that during the sintering process, a reaction between the americium oxide and spinel occurred to form a species with a perovskite structure. The identification of this species is being pursued. As it is likely that this species is an americium aluminate, by analogy with compounds produced by the reaction of Nd and Ce with spinel [6,7], the actual composition of the target probably was $MgAl_2O_4 + AmAlO_3$.

As $MgAl_2O_4$ is difficult to dissolve in aqueous media, the Am content of the pellets was determined by gamma spectroscopy measurements. Four gamma energies (59.5, 103.0, 125.3, 208 keV) were used, and the measurements were calibrated by measurements made on reference pellets with 8 wt% Am in spinel, which were prepared by mechanical mixing and blending of powders [5]. The Am content in the pellets was found to vary between 9.7 and 11.9 wt%, the mean value being 11.1 ± 0.7 wt%.

A representative pellet was sectioned in the axial direction and the Am distribution was determined by α-autoradiography, as shown in Fig. 1. The result indicates a less uniform Am distribution than found in pretests. A roughly cylindrically symmetrical shell, 200 μm thick, was observed, within which the Am content was higher than in the surrounding regions. These results have been further quantified using EPMA. Within the Am rich shell, the Am content was about 14 wt%, while in the surrounding regions, an Am content of about 9 wt% was found. This inhomogeneity may be related to a non-uniform porosity of the uninfiltrated pellets, or to a diffusion process during the thermal treatment in the steps involving liquid to solid Am nitrate, or Am nitrate to oxide conversion. The presence of the cylindrical shell was also observed in the optical micrograph of the pellet (see Fig. 1). This would indicate that the porosity within this americium-rich region is different than in the remainder of the pellet. The americium-containing particles have a diameter less than 3 μm (see Fig. 2).

The target pin contained 10 pellets that were loaded under a controlled inert atmosphere (He with $O_2 < 0.5\%$ and $H_2O < 10$ ppm) into a 15/15 Ti stainless steel

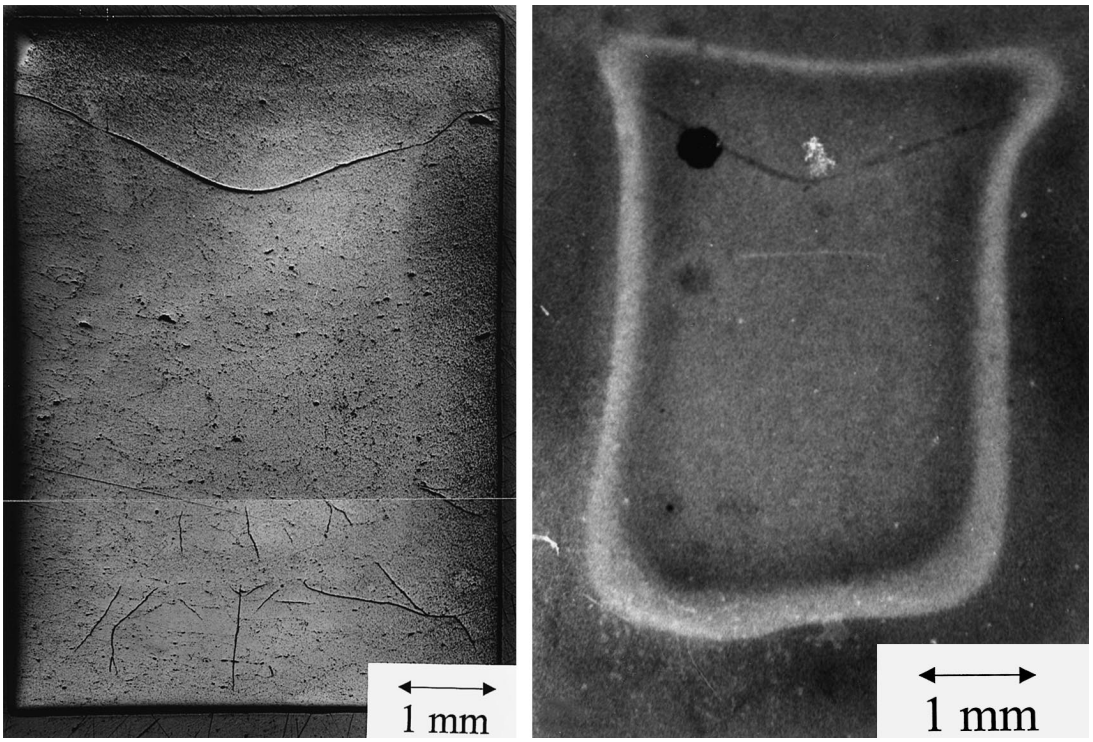

Fig. 1. Optical micrograph (left) and α-autoradiograph (right) of a representative pellet of the EFTTRA-T4 batch. The pellet diameter is 5.4 mm.

capsule (inner diameter 5.65 mm, outer diameter 6.55 mm). The target column (Am-spinel pellets) was 70 mm long and was terminated at each end by a $MgAl_2O_4$ pellet, with length, $l = 4.9$ mm, a Hf pellet ($l = 6.0$ mm) and a stainless steel pellet ($l = 17.0$ mm). The capsule was welded using the tungsten-inert-gas (TIG) method. The welds were inspected visually, tested non-destructively by X-ray radiography, and their seal was checked by means of a He leak test.

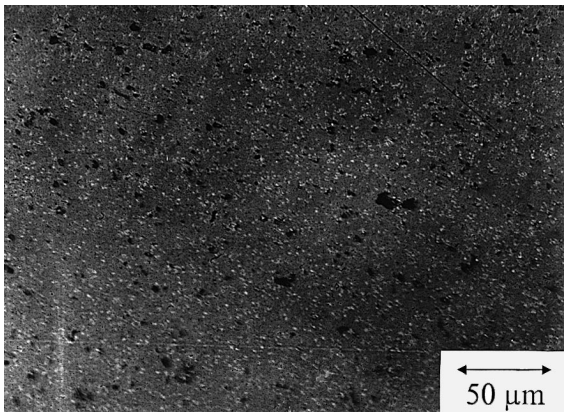

Fig. 2. Optical micrograph of a representative pellet of the EFTTRA-T4 batch. Particles that contain americium are observed as white features and have diameters less than 3 μm.

2.2. Irradiation

The EFTTRA-T4 sample was irradiated in the HFR Petten in a channel of a standard in-core TRIO-131 rig [8]. The EFTTRA-T4 sample holder consisted of three main sections. The lower in-pile section consisted of a stainless-steel containment, in which the target capsule and a variety of instrumentation monitors were mounted. These monitors were composed of 12 type-K thermocouples, four neutron fluence detector sets and four gamma-scanning wires (GSW1 to GSW4) and two capillary tubes for purging the containment with pure helium and for integrity check. The target capsule was positioned in a central hole of an aluminium carrier at centre-line core in the peak flux. The thermocouples were positioned at three levels around the target capsules. The fluence detector sets (which consisted of nickel-cobalt wire, iron wire, titanium wire, niobium wire and a piece of the gamma-scan wire) were located around the target capsule at the same radius as the thermocouples. The centre-line detector coincided with centre-line of the target stack. The four gamma scanning wires (a stainless steel wire of 1 mm thickness) were

located around the target capsule in 90° interval at a larger radius than the thermocouples. They extended over the entire length of the sample holder.

A shielding plug and a filter in the down-stream tube of the first containment formed the middle section of the sample holders. The filter, which had a length of 900 mm and a diameter of 8 mm, was filled with about 40 cm^3 activated charcoal. The filter served as a first in-pile barrier in case those gaseous fission products might be released from the target capsule in case of a failure.

The uppermost section of the sample holder consisted of a penetration plug with the dynamic O-ring sealing of the TRIO channel and the connectors for thermocouples and gas lines between sample holder and out-of-pile control panel. The sample holder was suspended at an extension rod with a snap connector for the coupling with a remotely operated vertical displacement unit (VDU). The dynamic sealing was required to achieve a high tightness of the TRIO channel during displacement of the sample holder. The maximum possible stroke of the sample holder was 150 mm.

The heat generated by fission and gamma absorption in the materials was radially dissipated through the structural materials and the gas gaps by conduction and radiation to the downstream primary water coolant at the surface of the TRIO channel. The required temperature distribution was realised by means of appropriately designed gas gap widths. For temperature adjustment, the gas gap between the first and second containment walls could be filled with adjustable mixtures of helium and neon that are stationary. The first containment was filled with pure helium. In addition, the axial temperature distribution could be adjusted by means of a vertical displacement unit that allowed movement of the target capsule in the vertical direction in order to keep it at the maximum neutron flux in spite of the setting of the control rods.

The irradiation lasted for a period of 14 HFR cycles, equivalent to 358.42 full power days. The first eleven cycles were performed in core position C5 and the last three cycles in core position C7, for core management reasons. The irradiation was interrupted after the first nine cycles (231 full power days) for the period of one cycle in order to inspect the target capsule by taking a neutron-radiograph image.

The temperature data are average values of the readings of 12 thermocouples, which were closely located around the target capsule. The temperature was maintained at about 400°C for all cycles, except for the first cycle where the temperature was maintained at 450°C. The higher temperature was justified by the low fission power of that cycle. As the irradiation progressed, the fission power increased to its maximum value during the last cycle. It should be noted that the specific gamma heating was about 30% lower during the last three cycles due to the change in core position.

2.3. Neutron metrology

Information about the neutron fluence distribution in the EFTTRA-T4 sample holder has been obtained from the analysis of the four gamma-scan wires (GSW) that were included in the sample holder. The following nuclear reactions that occur in this material have been analysed: (a) $^{50}Cr(n,\gamma)^{51}Cr$, (b) $^{58}Fe(n,\gamma)^{59}Fe$, (c) $^{59}Co(n,\gamma)^{60}Co$, (d) $^{58}Ni(n,p)^{58}Co$ and (e) $^{54}Fe(n,p)^{54}Mn$. Reactions (a) to (c) give information about the thermal-neutron fluence in the irradiation position, reactions (d) and (e) about the fast-neutron fluence. The bottom of the gamma-scan wires corresponds to a position 300 mm below the centre-core position of the HFR. This bottom position is the zero point of the measurement. The target capsule of the EFTTRA-T4 experiment was located between positions 145 and 390 mm, and the pellet stack between 200 and 270 mm. The gamma-scan wires have been analysed from 100 to 450 mm from the zero point. The results all show about the same fluence profile. An example is shown in Fig. 3. The maximum number of counts is found between 232 and 258 mm from the zero point of the gamma-scan wires, which is the location of the target capsule. The results show the neutron fluence profile has been fairly flat in the region where the target capsule was positioned. The buckling is about 2% over the length of the pellet stack.

The neutron-fluence detectors have been analysed by gamma spectrometry. In addition to the activation reactions (b), (c) and (e) shown above, the reactions $^{93}Nb(n,\gamma)^{94}Nb$, $^{46}Ti(n,p)^{46}Sc$ and $^{93}Nb(n,n')^{93m}Nb$ have been used to determine the neutron fluence. After the measurements, the results were processed by means of computer programs that yield activities, spectrum

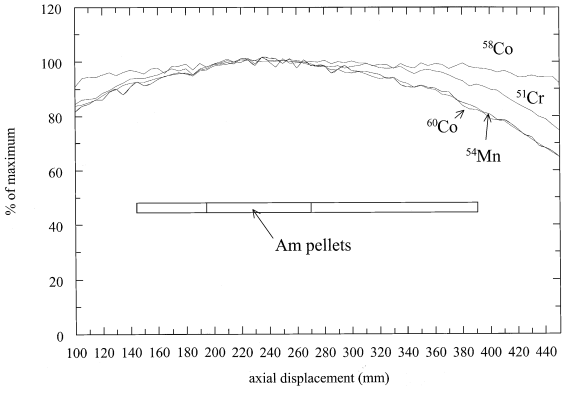

Fig. 3. Results of four nuclides for GSW1. The insert shows the approximate position of the T4 pellet stack.

Table 1
Results of the analysis of the neutron fluence monitors 1–4 (in m^{-2})

	Neutron fluence monitors			
	1	2	3	4
Thermal fluence (Co)	5.90×10^{25}	5.70×10^{25}	5.92×10^{25}	5.64×10^{25}
Fast fluence (Fe)	9.10×10^{25}	8.86×10^{25}	8.77×10^{25}	8.86×10^{25}
$E > 1.353$ MeV	6.66×10^{25}	6.49×10^{25}	6.42×10^{25}	6.49×10^{25}
67.4 keV $< E <$ 1.353 MeV	11.4×10^{25}	11.1×10^{25}	11.0×10^{25}	11.1×10^{25}
0.683 eV $< E <$ 67.4 keV	12.1×10^{25}	12.4×10^{25}	12.0×10^{25}	12.0×10^{25}
$E < 0.683$ eV	5.35×10^{25}	5.08×10^{25}	5.36×10^{25}	5.05×10^{25}
Total	35.5×10^{25}	35.1×10^{25}	34.8×10^{25}	34.6×10^{25}
$E > 0.1$ MeV	17.2×10^{25}	16.7×10^{25}	16.6×10^{25}	16.7×10^{25}
$E > 1$ MeV	8.22×10^{25}	8.01×10^{25}	7.92×10^{25}	8.01×10^{25}

indices and neutron fluence values.The main results are shown in Table 1. The thermal fluence has been derived from the $^{59}Co(n,\gamma)^{60}Co$ reaction, the fast fluence from the $^{54}Fe(n,p)^{54}Mn$ reaction. Also shown are the fluence values for the HFR-TEDDI group structure, and the fluences above 0.1 and 1 MeV.

3. Burn-up calculations

Detailed burn-up calculations for the EFTTRA-T4 experiment have been performed using the OCTOPUS burn-up code system of NRG [9]. The spectrum calculations were performed with the 3D Monte-Carlo code MCNP-4B [10] and the depletion calculations with the FISPACT-4 code [11]. The MCNP model has been restricted to the region around the core position C5, considering only the directly surrounding elements, which were cut in the vertical mid-plane. The leg of the TRIO facility containing the EFTTRA-T4 experiment has been modelled in detail; the other two legs of the TRIO facility have been homogenised as a mixture of aluminium and water. The fuel elements have been homogenised also and the boron-containing aluminium side plates have been modelled separately. The assembly has been enclosed by reflecting boundary conditions with reflecting coefficients to make k_{eff} equal to unity and to obtain the proper flux normalisation.

Four models for the americium pellets have been used:

A. Each of the 10 pellets is modelled as a cylinder with a homogeneous americium concentration equal to the average of all pellets.

B. Each of the 10 pellets is modelled as a cylinder with a homogeneous americium concentration equal to the actual average concentration in each pellet.

C. The pile of 10 pellets is modelled as a set of 10 concentric cylindrical zones with approximately equal ground surface. Zone 4 is the region with a larger Am concentration, the concentration ratio being 14:9 compared to the other zones.

D. A variation of model C, taking into account the effect of the top and bottom of the cylindrical shell with higher americium concentration.

The absolute flux normalisation for the depletion code FISPACT is based on the WIMS/HFR-TEDDI calculations for the actual core loading of each HFR cycle. The total cumulative neutron fluence in the calculations was 3.5×10^{26} m^{-2}. In the calculations, it was assumed that the experiment remained in position C5 during all cycles, which was not the case for the last three cycles when the sample was moved to position C7. With a 3D full core calculation it was checked that the flux spectra of positions C5 and C7 have the same shape and only differ by their normalisation. For the depletion calculation re-normalisation of the total flux was applied to take this effect into account.

The calculated flux distributions in the target, for which the statistical uncertainty is at the 1% level, show that the flux is essentially evenly distributed over the americium-containing pellets, with a slight buckling as was also observed in the gamma-scan wires. In the radial direction, the flux decreases by about 8% towards the centre of the pellets at the beginning of irradiation (model D). At the end of irradiation, this effect has been reduced to 3%.

The results of the burn-up calculations are shown in Table 2. They indicate that the extent of transmutation of americium ^{241}Am is about 96%, the ^{241}Am being transformed mainly to ^{238}Pu and ^{242}Cm (see Fig. 4). The extent of fission, the actual measure for the destruction of the actinides, is 28%. Also shown in Table 2 is the actinide composition one year after the end-of-irradiation (EOI). This corresponds to the time of puncturing of the target capsule (21 January 1999). It can be seen that at this time the amount of ^{242}Cm has been reduced by about 80% as a result of the alpha decay to ^{238}Pu (Fig. 4).

Table 2
Composition of the main actinide isotopes in the EFTTRA-T4 target as obtained by post-test MCNP/FISPACT calculations, expressed as the fraction (in %) of the initial amount of ^{241}Am

	Initial (%)	Final (%)	
		End-of-irradiation	EOI + 1 year
^{241}Am	100	3.7 ± 0.2	3.8 ± 0.2
^{243}Am		5.1 ± 0.2	5.1 ± 0.2
^{238}Pu		24.1 ± 0.1	36.3 ± 0.1
^{239}Pu		6.5 ± 0.1	6.5 ± 0.1
^{242}Pu		7.4 ± 0.5	7.5 ± 0.5
^{242}Cm		15.6 ± 0.1	3.1 ± 0.1
Total actinides	100	72.1 ± 0.2	72.1 ± 0.2

4. Results

4.1. Non-destructive examinations

Visual inspection of the target pin did not show any irregularities following irradiation. The welds at the bottom and the top of the capsule were intact. Also X-ray radiography of the target pin did not reveal any irregularities. From the distance between the hafnium pellets, which are clearly visible on the radiograph, the length of the pellet stack was measured (see Table 3). The value obtained (82 mm) is somewhat larger that the original stack length (80.4 mm). These observations confirm the results of the neutron radiography measurement made in 1997 after 231 full power days, which also indicated an increase in the pellet stack. Careful image analysis of the neutron radiography also allowed to determine the length of the ten pellets as 72.2 mm, compared to 70.6 mm before irradiation.

Fig. 5 shows the axial distribution of three radionuclides along the capsule as obtained by gamma scanning. The activity curve of ^{51}Cr, an activation product of the steel, clearly shows the positions of the components of the capsule, the top and bottom plugs, the steel cylinders, the hafnium pellets, the spinel pellets, the americium-containing pellets and the Inconel spring. The rather flat profile of ^{51}Cr along the pellet stack confirms the measurements of the gamma-scan wires indicating that the neutron fluence was also flat. The hafnium pellets are clearly visible by the strong intensity of ^{181}Hf, the activation product of the natural hafnium ^{180}Hf isotope present in the two pellets. The distance between the hafnium pellets derived from this measurement confirms the observation from neutron and X-ray radiography, i.e. the length of the pellet stack has increased by 4–5%. The pellet stack is characterised by the sharp increase of the activity of the fission products, as shown here by ^{95}Zr.

The activities of the fission products all exhibit the same irregular shape along the stack length as it is shown for ^{95}Zr. This includes the mobile fission products

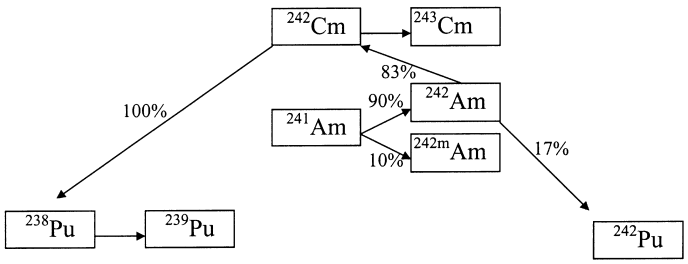

Fig. 4. Transmutation scheme for ^{241}Am in a thermal flux.

Table 3
Dimensional changes of the pellets of the T4 test derived indirectly from non-destructive examinations. The pellet stack length refers to the distance between the two Hf pellets

	Time (full power days)	Stack length		Pellet diameter	
		(mm)	δ (%)	(mm)	δ (%)
Loading	0	80.4	–	5.39	–
Neutron radiography	231.4	84.5	+5.2		
Gamma spectrometry	358.4	84.0	+4.5	5.75	+6.7
Gamma tomography	358.4			5.75	+6.7
X-ray radiography	358.4	82	+2		
Profilometry				5.75[a]	+6.7

[a] Maximum value.

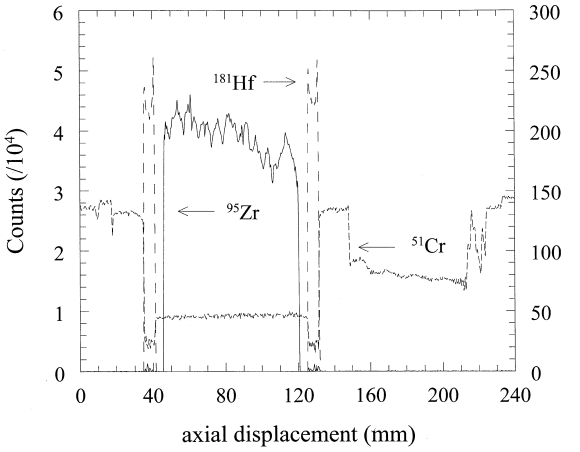

Fig. 5. Axial distribution of three radionuclides along the target capsule. The activation product ^{51}Cr of the steel, the activation product ^{181}Hf of the hafnium pellets and the fission product ^{95}Zr.

like iodine (^{131}I) and cesium (^{134}Cs and ^{137}Cs) which are shown in Fig. 6. The general trend in these curves can be correlated to the initial americium concentration in the pellets, as shown in Fig. 7. In this figure, the original height of the pellets has been corrected for the increase in length as observed at the end of the irradiation. It is clear that the higher the initial americium content the higher is the ^{141}Ce activity in the pellets. However, two maxima and one minimum occur within each pellet. This can be explained by the inhomogeneous initial distribution of ^{241}Am in the pellets. The maximum values occur close to the top and the bottom of the pellets where the slice of the 14 wt% zone opposes the detector, the minimum occurs in the centre of the pellets, where the effect of this slice is the smallest.

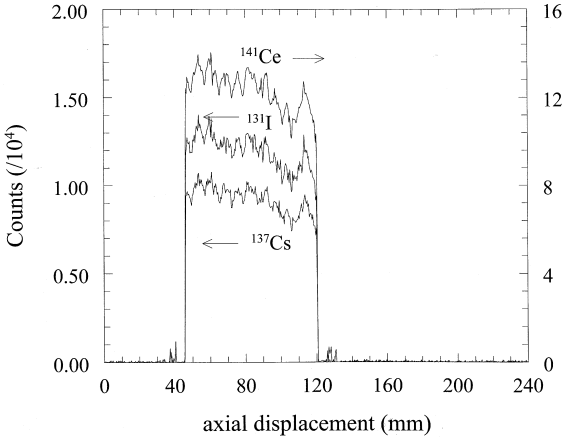

Fig. 6. Axial distribution of the radionuclides ^{131}I, ^{137}Cs and ^{141}Ce along the target capsule.

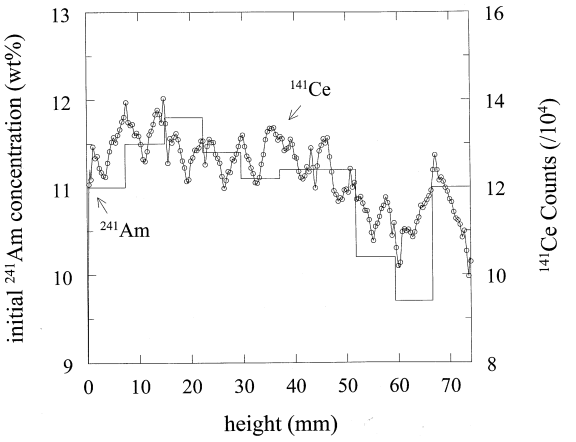

Fig. 7. Axial distribution of the fission product ^{141}Ce along the pellet stack as obtained by gamma spectrometry (○) and the initial ^{241}Am concentration in the pellets (solid line).

The gamma tomography of the fission products also shows this inhomogeneous distribution of the initial americium concentration (Fig. 8). The tomography also revealed that the diameter of the pellets was about 5.75 mm after irradiation, which is about 6% larger than the initial value. A radial gamma scan recorded with a higher accuracy has confirmed this value.

The value 5.75 mm for the diameter of pellets is larger than the inner diameter of the cladding tube (5.65 mm) before the irradiation. Expansion of the cladding must therefore have occurred and has been confirmed by profilometry analysis (Fig. 9). The maximum outer diameter of the cladding tube (6.75 mm) occurs in the region where the americium-containing pellets are positioned. This value has to be compared to 6.55 mm prior to the irradiation. Assuming that the thickness of the cladding tube is marginally affected by the swelling, the maximum pellet diameter is calculated to be 5.85 mm. The profile of the cladding in the region where the americium-containing pellets are positioned shows the same pattern correlated to the initial Am concentration, as observed in the gamma scans for the fission products.

4.2. Gas puncturing

The gas puncturing yielded a pressure of 0.5 MPa (5 bar) and a free volume of 1.76 cm^3. The measurement of the composition by mass spectrometry resulted in the following volume fractions: 0.9492 for helium, 0.0303 for xenon and 0.0027 for krypton. The remaining fraction 0.0178 was composed of N_2, O_2, Ar and CO_2. Judging from the relative amounts of the latter gases, they are most likely impurities present during the filling of the target pin. The isotopic masses of the fission gases

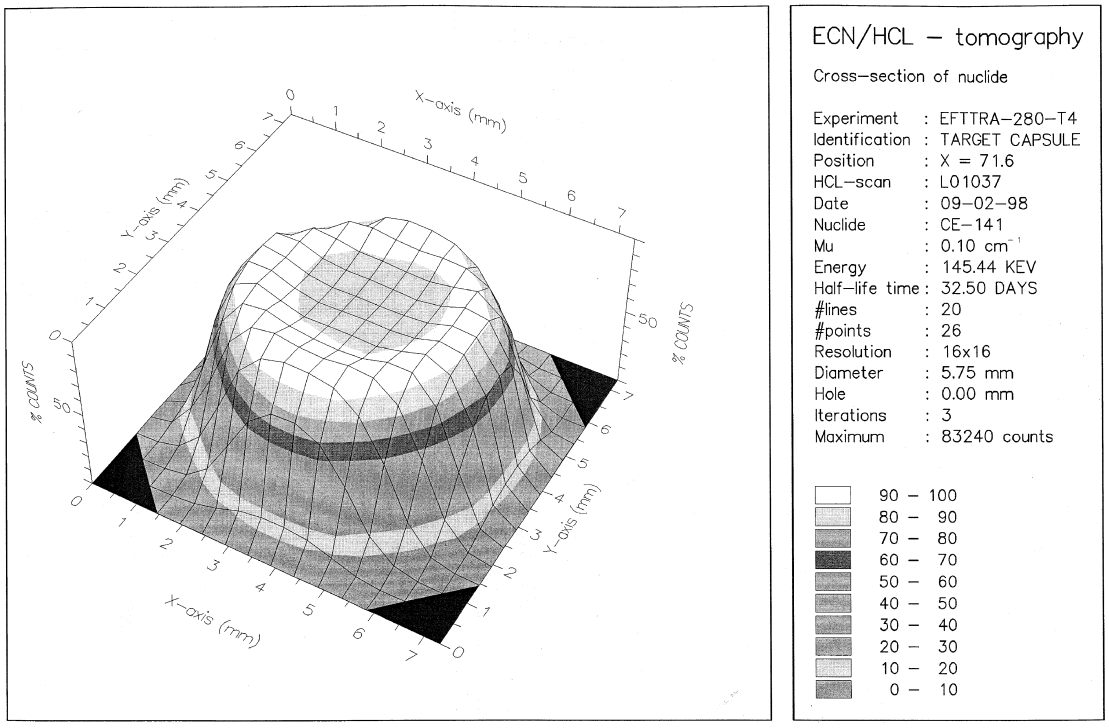

Fig. 8. The distribution of ^{141}Ce in the EFTTRA-T4 pin obtained by gamma tomography.

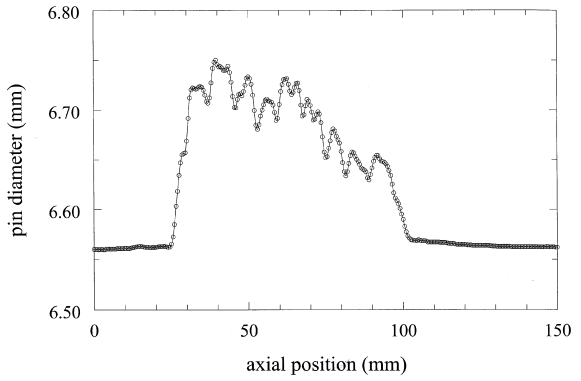

Fig. 9. The diameter of the cladding of the irradiated T4 rod (original diameter 6.55 mm).

as well as helium, obtained from the measurements, are shown in Table 4. When these values are compared to the isotopic masses obtained by the post-test MCNP calculations, is it found that the released fraction of helium is 20% (assuming that the helium produced during the one year cooling of the pin is retained in the pellets) and that of the fission gases 5%. The released fraction for the Xe and Kr isotopes are, however, distinctly different. This might partially be due to the fact that the measured concentrations of the Kr isotopes are close to the detection limit of the measurement device. Therefore, the Xe release fractions considered are much more reliable.

4.3. Destructive examinations

After the non-destructive examinations of the T4 rod, a ceramographic sample was made at the maximum activity position according to the axial gamma scanning. After cutting, the sample was embedded in resin and polished. A macrograph of the polished sample is shown in Fig. 10. Two main features can be observed:

1. As expected from the profilometry measurements, the gap between pellet and cladding is completely closed. Crack healing phenomena can also be seen, indicating a strong pellet/cladding interaction as the result of the swelling of the pellet (see discussion below).
2. At the position $r/r_0 \simeq 0.7$ a band, about 350 μm wide, can be observed. This band, shown in more detail in Fig. 11, is characterised by a significantly higher porosity than in the remainder of the sample and probably coincides with the zone with higher Am content present in the unirradiated samples as described in Section 2.1.

The typical porosity at different radial positions in the pellet is shown in Fig. 12. At position $r/r_0 \simeq 1$, the rim of the pellet, mainly spherical porosity (gas bubbles) can be seen, uniformly spaced in the matrix. Almost no

Table 4
Results of the gas puncturing of the EFTTRA-T4 target pin. The calculated inventory is based on the results of the MCNP-FISPACT calculations

	Mass (mol)		Fraction released (%)[a]
	Released	Inventory[b]	
^{4}He	2.66×10^{-4}	1.37×10^{-3}	19.5
Fission gases (total)	1.19×10^{-5}	2.29×10^{-4}	5.2
^{83}Kr	9.92×10^{-8}	1.04×10^{-6}	9.5
^{84}Kr	4.13×10^{-7}	2.56×10^{-6}	16.1
^{85}Kr	6.74×10^{-8}	7.81×10^{-7}	8.6
^{86}Kr	4.86×10^{-7}	4.54×10^{-6}	10.7
^{131}Xe	5.57×10^{-7}	1.79×10^{-5}	3.1
^{132}Xe	2.51×10^{-6}	4.79×10^{-5}	5.2
^{134}Xe	2.66×10^{-6}	5.23×10^{-5}	5.1
^{136}Xe	5.12×10^{-6}	1.02×10^{-4}	5.0

[a] Released mass divided by the inventory for each nuclide.
[b] End of irradiation.

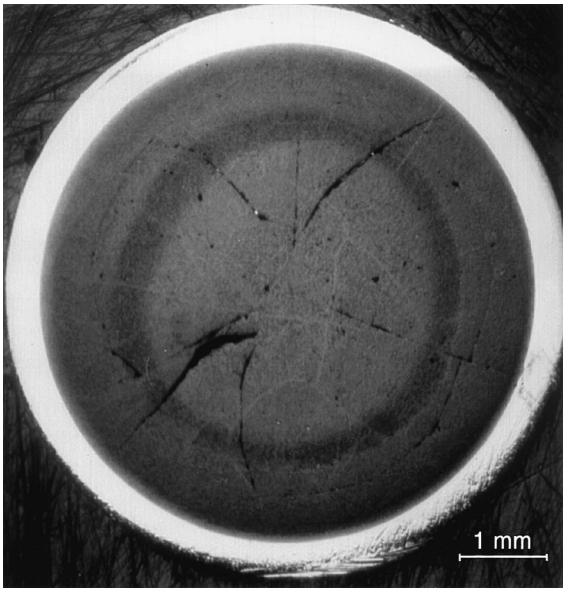

Fig. 10. Macrograph of the T4 sample.

linkage of pores can be observed. The lower porosity in the immediate vicinity of the cladding is probably due to the increased stress field caused by the pellet/cladding interaction. The porosity at the centre side of the high-porosity band consists of larger pores than that in the region towards the cladding. This trend of larger and more separated pores towards the centre of the pellet is confirmed at position $r/r_0 \simeq 0$ and reveals the influence of the central temperature of the sample during irradiation.

The porosity of the sample was measured by image analysis in the different zones of interest, namely at the periphery, at the centre and at the high porosity band.

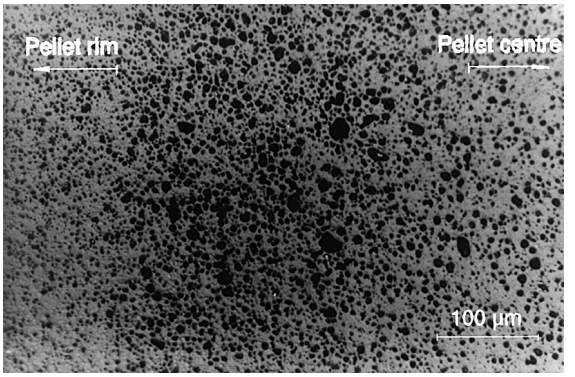

Fig. 11. High-porosity band of about 350 μm.

The total porosity was about the same at the periphery and at the centre of the sample: 16% (area fraction). In contrast, in the high-porosity zone, the measurements reveal a porosity of 40% (area fraction). These values lead to an overall porosity of about 18%, compared to a mean initial porosity of the unirradiated pellet of 3%. In the periphery of the sample, pores of 1.4 μm in mean diameter are found, whereas in the centre and in the high porosity band, pores of about 4.5 μm in mean diameter are predominant.

5. Discussion

The results presented in the previous section indicate that considerable swelling (up to 18% in volume) of the pellets occurred. The swelling of the pellets was constrained by the cladding, as the gap between pellet and cladding was closed and the cladding deformed. As a result, evidence for crack healing during irradiation could be observed.

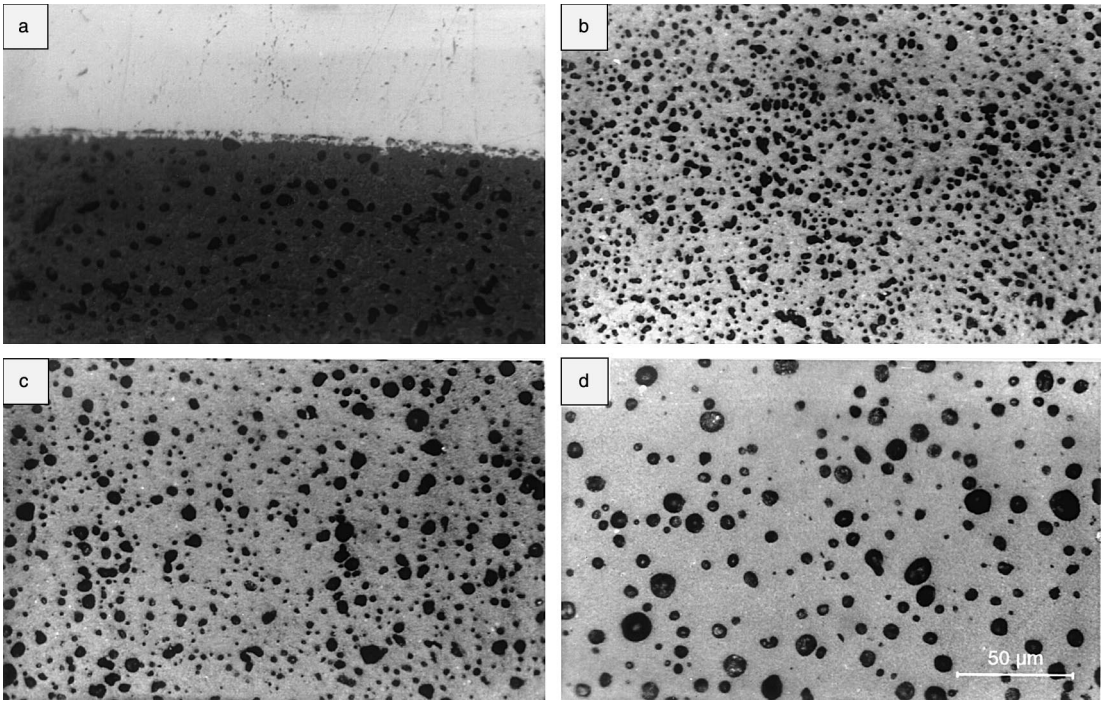

Fig. 12. Ceramographies showing the porosity at: (a) pellet rim ($r/r_0 = 1$), (b) the side of the high-porosity zone towards the pellet rim, (c) the side of the high-porosity zone towards the centre, and (d) at pellet centre ($r/r_0 = 0$).

The swelling of the pellets can be caused by two different processes: (i) the damage of the $MgAl_2O_4$ matrix by fission fragments, and (ii) the accumulation of helium produced by the alpha decay of ^{242}Cm, one of the isotopes in the transmutation chain of ^{241}Am (see Fig. 4). The effect of damage to the matrix caused by neutron irradiation can be neglected as irradiation experiments performed on $MgAl_2O_4$ under almost the same irradiation conditions as in the HFR, do not show any significant effect [12,13].

Ion implantation experiments have shown that $MgAl_2O_4$ is also very resistant to ion irradiation, even at high ion doses [14]. However, these experiments were made with ions of energies that are well below the fission energy. Recent experiments [15] with ions of fission energy (72 MeV iodine ions) showed that the stopping of the heavy ions can damage of the magnesium aluminate spinel, eventually resulting in amorphisation. The extent of damage depends upon the temperature of the sample and was quantified in terms of volume increase (swelling) of the matrix. At room temperature a linear swelling of more than 20% was observed at the sample surface, while at 1200°C no swelling was observed. For single crystals, the swelling saturates with increasing ion fluence at all temperatures. The damage is caused by the energetic heavy ions, which, like the fission fragments in nuclear fuels, cause damage tracks of about 8–10 μm in length. As the size of the americium-containing particles in the T4 experiment is only 2–3 μm and the distance between the particles is less than 10 μm, the volume of the $MgAl_2O_4$ matrix subjected to fission product damage will be close to 100%.

The helium produced by alpha decay will also cause damage of the matrix. However, this damage is negligible compared to that caused by the fission products because it consists mainly of isolated displacements along the range of the alpha particle (20 μm) [16,17]. However, helium is an inert gas with a high diffusion coefficient and a low solubility in most ceramic materials. The diffusion of rare gases such as helium in ceramics is a complex process involving several rate-determining mechanisms. Helium can diffuse as an atom in the matrix and accumulate in gas bubbles in grains or at grain boundaries. The formation of gas bubbles and the concomitant pressure build-up will increase the porosity in the material and will eventually result in swelling. At sufficiently high concentration at the grain boundaries the gas bubbles can combine, and eventually form paths for gas release. The extent of helium mobility will depend upon the diffusion rate, which in turn will depend upon the temperature. It is generally accepted that at low temperature, atomic diffusion is the dominant mechanism, at high temperatures gas bubble migration is the dominant process. In addition, radiation damage will strongly influence these diffusion mechanisms.

It is thus clear that the temperature of the pellets is an important parameter for radiation damage as well as for helium accumulation. However, the exact temperature and temperature distribution of the T4 pellets is not known. It was not measured, but calculated from the geometry and power evolution and estimated material properties such as thermal conductivity. However, the closure of the gas gap between pellet and cladding and between the cladding and the aluminium container will have a strong impact on the temperature. Also the differences in the americium concentration of the individual pellets, which was not taken into account for the power calculations, and the strong increase in the porosity of the pellets are effects not included in the calculations. The effect of the inhomogeneous americium concentration within each pellet probably can be neglected. Since the magnitude of these effects cannot be quantified easily, the maximum temperature the fuel pellets reached is not clear.

As the extent of swelling of the pellets is proportional to the initial americium concentration of the 10 pellets, as shown by the profilometry measurements, the process determining the swelling probably was continuous and did not reach a saturation level. This indicates that the accumulation of helium in gas bubbles was probably the predominant process causing the swelling of the T4 pellets, since the effect of ion damage should have reached a saturation level [15]. This conclusion is confirmed by ceramographic analysis, which indicates that the increase of porosity due to gas bubble formation is in the order of 15%, very close to extent of swelling.

The helium release for the T4 experiment is about 20%. This means that about 80% of the helium atoms are still present in the pellets, either in gas bubbles or as atoms or clusters of atoms in the lattice. The fission gas release found experimentally is 5%, which is four times lower than the helium release. This difference can be explained by the higher diffusion coefficient of the small helium atoms compared to the much larger xenon atoms. It has been suggested that the diffusion coefficient of He in UO_2 is 10^3 times higher than that of xenon [18]. A factor of 3–4 between helium and fission gas release has also been found for mixed oxide (MOX) fuel [18,19].

6. Conclusions and outlook

From the results of the EFTTRA-T4 experiment, as described in the present paper, the following conclusions can be drawn:

- The fabrication campaign for the T4 target has demonstrated the feasibility of using the infiltration technique for the fabrication of inert-matrix targets containing americium. The infiltration technique can be automated, it is compatible with remote handling, and produces minimal quantities of dust and waste, as required for the production of minor actinide targets. However, further development is required to eliminate the possibility of inhomogeneities of the Am distribution in the pellets, as was observed in the T4 experiment.
- The T4 target has been irradiated successfully during 358 full power days in the HFR at Petten. During this period, an extent of actinide transmutation of 94% and of actinide fission of 28% was achieved, as derived from post-test calculations.
- Post-irradiation examinations have shown that the T4 target pellets have swollen considerably (up to 18%). This can be attributed to the accumulation of helium (produced by alpha decay of ^{242}Cm) in gas bubbles, which has played a much more important role than anticipated. The post-irradiation examinations revealed no evidence for bubble migration at the relatively low operating temperatures of the T4 target.
- The accumulation of helium is an intrinsic problem of americium transmutation in reactor fuels or targets, and is only partially related to the choice of the matrix.

The latter conclusion is of major importance for the outlook on americium transmutation and has to be taken into account in the design of fuels and targets for Am transmutation. However, recent concepts for heterogeneous targets [16] mainly deal with the minimisation of effects the radiation damage. To achieve this, a dispersion of $(Zr, Y, Am)O_{2-x}$ host particles with a size between 50 and 300 μm in an inert matrix has been suggested because the damage will then be restricted almost completely in the host particle [20–22]. In that case the helium gas (and the fission gases) will accumulate in the host particle and at the interface of the host particle and the matrix. Eventually this could also lead to swelling, especially at high burnup when destruction of grains can be expected and the contained gas is released from the host phase, as it is the case in MOX produced by the MIMAS process. Technical solutions must therefore be found to deal with this problem, for example by inclusion of tailored porosity to accommodate swelling or provide channels for release, by decreasing the smeared density of the fuel to permit pellet swelling, or, more drastically, by using non-pellet type designs such as sphere-pac fuels or targets.

Acknowledgements

The authors wish to acknowledge the assistance of D. Dams (JRC-IAM) for the irradiation, J.C. Closset, A. Fernandez, C. Fuchs, R. Voet, K. Richter, J.F. Gueugnon and J. McGinley (JRC-ITU) for the technical assistance for the fabrication of the target; A. Stalios

(JRC-ITU) for the technical assistance for the ceramographies; J.L. Kloosterman (IRI Delft) for his reactor-physics support; K. Bakker (NRG) for thermal calculations; H. Buurveld and J. Minkema (NRG) for the technical assistance for the post-irradiation examinations; C. Sciolla (NRG) for the pre-irradiation nuclear calculations; A. Paardekooper (NRG) for the neutron metrology analysis. In addition, the authors wish to the Commission of the European Communities (DGXII) for the financial support of the project (contract no. FI4I CT95-007), and M. Hugon, the responsible scientific officer at DGXII, for his interest and support.

References

[1] C. Madic, M.J. Hudson, J.-O. Liljenzin, J.-P. Glatz, R. Nannicini, A. Facchini, Z. Kolarik, R. Odoj, in: Proceedings of the Fifth International Information Exchange Meeting on Actinide and Fission Product Partitioning and Transmutation, Mol, Belgium, 25–27 November 1998, p. 53.

[2] J.L. Kloosterman, E. Kiefhaber, M. Rome, J. Tommasi, Proceedings GLOBAL'97, Yokohama, Japan, 5–10 October 1997, p. 338.

[3] J.F. Babelot, R. Conrad, W.M.P. Franken, J. van Geel, H. Gruppelaar, G. Mühling, C. Prunier, M. Rome, M. Salvatores, Proceedings GLOBAL'95, 11–14 September 1997, Versailles, France, vol. 1, p. 524.

[4] J.F. Babelot, R. Conrad, H. Gruppelaar, G. Mühling, M. Salvatores, G. Vambenepe, Proceedings GLOBAL'97, 5–10 October 1997, Yokohama, Japan, vol. 1, p. 676.

[5] K. Richter, A. Fernandez, J. Somers, J. Nucl. Mater. 249 (1997) 121.

[6] A. Fernandez, J. Somers, unpublished results.

[7] R.J.M. Konings, K. Bakker, J.G. Boshoven, H. Hein, M.E. Huntelaar, J.D. Meeldijk, C.F. Woensdregt, H. Zhang, in: Proceedings of the International Conference on Future Nuclear Systems, Global 97, 5–10 October, Yokohama, Japan, p. 670.

[8] J. Ahlf, A. Zurita, Commission of the European Communities, Report EUR 15151 EN, 1993.

[9] J.L. Kloosterman, J.C. Kuijper, P.F.A. de Leege, Energieonderzoek Centrum Nederland, Report ECN-RX–96-032, 1998.

[10] J.F. Briesmeister (Ed.), MCNP, a general Monte Carlo Code for neutron and photon transport, versions 4A and 4B. Los Alamos National Laboratory, New Mexico, USA.

[11] R.A. Forrest, J.Ch. Sublet, FISPACT 4 User manual. EASY Documentation series UKAEA FUS 287. UKAEA, April, 1995.

[12] R.J.M. Konings, K. Bakker, R. Conrad, C. Boshoven, H. Hein, J. Nucl. Mater. 254 (1998) 135.

[13] E.A.C. Neeft, R.J.M. Konings, J.G. Boshoven, H. Hein, R.P.C. Schram, K. Bakker, A. van Veen, R. Conrad, J. Nucl. Mater. 274 (1999) 78.

[14] L.M. Wang, W.L. Gong, N. Bordes, R.C. Ewing, Y. Fei, Mater. Res. Soc. Symp. Proc. 373 (1995) 407.

[15] T. Wiss, Hj. Matzke, Rad. Measure. 31 (1999) 507.

[16] N. Chauvin, R.J.M. Konings, Hj. Matzke, J. Nucl. Mater. 274 (1999) 105.

[17] R. Fromknecht, J.-P. Hiernaut, Hj. Matzke, T. Wiss, Nucl. Instrum. and Meth. 166&167 (2000) 263.

[18] K. Kamimura, Y. Kobayashi, T. Nomata, in: Proceedings International Symposium on MOX Fuel Cycle Technologies for Medium and Long Term Deployment: Experience, Advances, Trends, Vienna, 17–21 May 1999.

[19] K. Katsuyama, T. Mitsugi, T. Asaga, Trans. ANS 66 (1998) 115.

[20] N. Chauvin, J. Tomassi, V. Georgenthum, G. Ritter, in: Proceedings Global'97, Yokohama, October 1997, p. 690.

[21] K. Bakker, R.J.M. Konings, J. Nucl. Mater. 254 (1998) 129.

[22] K. Bakker, R.J.M. Konings, J. Alloys Comp. 271–273 (1998) 632.